Time–Frequency Analysis of Power Quality Signals: A Novel Amplitude-Preserving Adaptive Synchrosqueezed S-Transform

Time-Frequency Analysis of Power Quality Signals: A Novel Amplitude-Preserving Adaptive Synchrosqueezed S-Transform

Kunzhi Zhu, Zhaosheng Teng, Alessandro Mingotti *Member, IEEE,* Qiu Tang, Lorenzo Peretto, *Senior Member, IEEE,*

***Abstract*—With the widespread deployment of renewable energy and power electronic devices, the incidence of power quality disturbances (PQDs) has risen significantly. This paper presents a novel approach for accurately detecting the parameters of PQDs: an amplitude-preserving adaptive synchrosqueezed S-transform. Firstly, to mitigate computational burden, a fast calculation method for the instantaneous frequency (IF) is introduced. This method efficiently separates the real and imaginary parts of complex numbers, reducing unnecessary computations and preserving information integrity at the edges of the IF matrix. Secondly, to counter the impact of changes in window width on the accuracy of PQDs amplitude detection, a synchrosqueezed S-transform framework with amplitude preservation is proposed. Furthermore, to accommodate the detection requirements of various signal components within PQDs signals, an amplitude-preserving adaptive synchrosqueezed S-transform (APASST) is introduced. This method ensures amplitude accuracy post-synchrosqueezing through normalization windows in the frequency domain, facilitating the accurate detection of multiple PQDs signal components via adaptive adjustment. Finally, the simulation and experimental results prove the efficacy of the proposed method.**

***Index Terms*—Power quality disturbance, Time-frequency analysis, Synchrosqueezed S-transform, Instantaneous frequency, Amplitude-preserving adaptive window.**

I. Introduction

In recent years, the share of renewable energy sources (RES) in the energy mix has experienced rapid growth [1]. However, their inherent instability, coupled with the widespread adoption of power electronic devices, inevitably introduces power quality disturbances (PQDs) into the power grid. Furthermore, the proliferation of electric vehicle charging stations adds to the prevalence of power quality disturbances [2]. PQDs not only compromise the reliability of power supply but also pose potential economic losses [3]. Hence, accurate detection of power quality disturbance parameters is imperative for effective control of power quality and for the management of the network.

While Fourier transform (FT) and its variants have traditionally been employed to discern the frequency characteristics of power systems [4], they prove inadequate for analyzing non-stationary signals. Modal decomposition techniques, such as ensemble empirical mode decomposition (EEMD) [5] and variational mode decomposition (VMD) [6], break down non-stationary signals into multiple inherent modal functions, offering features for PQDs classification. However, detecting PQD parameters through these decomposed functions is challenging due to modal aliasing and endpoint effects.

In contrast, time-frequency analysis emerges as a more suitable approach for PQD's parameter analysis, as it provides both time and frequency domain insights. Short-time Fourier transform (STFT) utilizes a sliding window to capture time-frequency information [7], yet its fixed window width limits time-frequency resolution. Wavelet transform (WT) offers variable time-frequency resolution, yet selecting an appropriate wavelet function demands expertise, and converting the time-scale distribution to obtain the time-frequency distribution (TFD) adds complexity [8]. Compared with STFT and WT, the Stockwell transform (ST) emerges as a more flexible option for adjusting time-frequency resolution, directly yielding TFD without the need for conversion [9]. The original ST has two main ways to improve performance, namely use different window functions and change the control strategy for window width. The S-transform with digital prolate spheroidal window (PSWST) replaced Gaussian window [10], adaptive kaiser S-transform (AKST) uses kaiser window [11], and asymmetrical kaiser window-based S-transform (AKWST) uses asymmetric window [12]. The frequency form of unscaled S-transform (FUST) uses a fixed window width [13], the improved S-transform (IST) uses two parameters to control the width of the window [14], optimized S-transform (OST) uses three parameters [15], and modified S-transform (MST) uses four parameters [16], etc.

However, despite these advancements, achieving high time and frequency resolution simultaneously remains a challenge. The reassignment method (RM) aims to enhance the energy concentration of TFD by relocating it to the ridge position, but it does not reconstruct the signal [17]. Synchrosqueezed wavelet transforms (SWT) identify signal component ridge

This work was supported in part by the National Natural Science Foundation of China under Grant 52077067, and in part by the Hunan Natural Science Foundation under Grant 2021JJ30124. (Corresponding author: Zhaosheng Teng.)

Kunzhi Zhu is with the College of Electrical and Information Engineering, Hunan University, Changsha 410082, China, and also with the Department of Electrical, Electronic and Information, University of Bologna, 40136 Bologna, Italy (e-mail: zhukunzhi@hnu.edu.cn).

Zhaosheng Teng and Qiu Tang are with the College of Electrical and Information Engineering, Hunan University, Changsha 410082, China (e-mail: tengzs@hnu.edu.cn; tangqiu@hnu.edu.cn).

Alessandro Mingotti and Lorenzo Peretto are with the Department of Electrical, Electronic and Information, University of Bologna, 40136 Bologna, Italy (e-mail: alessandro.mingotti2@unibo.it; lorenzo.peretto@unibo.it).

lines through instantaneous frequency (IF), redistributing energy to improve the energy concentration of the time-scale distribution [18]. Nevertheless, SWT still relies on manual selection of wavelet functions and requires transformation of the time-scale distribution into a time-frequency distribution. Synchrosqueezed transforms based on STFT exhibit improved performance over STFT alone, yet their time-frequency resolution remains fixed [19] [20]. T he s ynchrosqueezed S-transform (SST) retains the benefits o f t he S -transform and finds w idespread u se i n I F e stimation f or a pplications such as seismic time-frequency analysis and fault diagnosis [21] [22] [23]. Additionally, for extracting the IF of highly time-varying signals, second-order or higher-order synchrosqueezed transforms have been proposed [24] [25] [26] [27] [28], albeit at the expense of increased computational complexity.

As the SST involves calculating the IF matrix and conducting synchrosqueezing operations, it imposes additional computational burden. The change in window width of the ST impacts the amplitude of the TFD post-synchrosqueezing, thereby affecting the accuracy of PQDs parameter detection. While the time resolution of SST improves with frequency, the primary characteristic of PQDs lies in their time-varying amplitude at the power frequency. Motivated by these factors, this paper proposes a novel amplitude-preserving adaptive synchrosqueezed S-transform (APASST) to enhance the accuracy of PQD's parameter detection. The contributions of this work are outlined as follows:

1) Introducing a new method for calculating instantaneous frequency to reduce computational burden. This method utilizes Fourier's differential theorem to compute the derivative of ST, thus preventing information loss at the edges. Furthermore, unnecessary computational burden during IF calculation is minimized by segregating the real and imaginary components of complex numbers.
2) Proposing an amplitude-preserving SST (APSST) to counter the impact of ST window width changes on post-synchrosqueezing amplitude. APSST employs a correction factor to ensure the sum of the window in the frequency domain equals to 1, thereby preserving the accuracy of TFD amplitude after synchrosqueezing. Different from existing approaches, APSST can provide accurate amplitude mapping of different signal components.
3) Presenting an amplitude-preserving adaptive SST (APASST) based on APSST to accurately detect PQDs parameters. APASST offers robust time-frequency resolution across both low and high frequencies, facilitating improved parameter detection of PQDs. Additionally, parameter selection methods for APASST are provided.
4) Validating the performance of APASST through extensive experimentation. Simulation and experimental tests conducted on a PQD analysis platform demonstrate that APASST achieves high accuracy in detecting both single and complex PQDs.

The subsequent sections of this paper are structured as follows: Section II outlines the fast calculation method of IF and introduces APSST. Section III focuses on APASST and its discrete algorithm. Section IV presents the experimental results, while Section V concludes the paper.

II. The basic theory of APSST

A. The Stockwell Transform

Let $\mathbb{R}$ denote the set of real numbers, $L^2(\mathbb{R})$ represents a square-integrable function space of $\mathbb{R}$. For time domain signals $x(t) \in L^2(\mathbb{R})$, the ST of $x(t)$ is:

$$ST(\tau, f) = \int_{-\infty}^{+\infty} x(t) w(\tau - t, f) e^{-j2\pi f t} dt, \tag{1}$$

where, $w(t, f)$ is a Gaussian window, $w(\tau - t, f)$ is the time shift of $w(t, f)$. $w(t, f)$ is defined as:

$$w(t, f) = \frac{1}{\sqrt{2\pi}\sigma(f)} e^{-\frac{t^2}{2\sigma(f)^2}}. \tag{2}$$

In (2), the value of $\sigma(f)$ changes with frequency to obtain various time-frequency resolutions. According to Plancherel theorem, $ST(\tau, f)$ can be calculated in frequency domain through:

$$ST(\tau, f) = \int_{-\infty}^{+\infty} X(f + \beta) W(\beta, f) e^{j2\pi\beta\tau} d\beta, \tag{3}$$

where, $X(\beta)$ and $W(\beta, f)$ are the Fourier transforms of $x(t)$ and $w(t, f)$, respectively. $W(\beta, f)$ is defined as:

$$W(\beta, f) = e^{-2\pi^2\beta^2\sigma(f)^2}. \tag{4}$$

B. A new perspective for the SST

Refer to the definition of narrow-band intrinsic mode functions (IMF) in [18], a narrow-band IMF signal can be defined as:

$$x_0(t) = A_0(t) cos(\phi_0(t)), \tag{5}$$

where, the variation of $A_0(t)$ and $\phi_0'(t)$ is much slower than that of $\phi_0(t)$ [18]. Considering that the ST is based on FT, $x_0(t)$ can be written in the form:

$$x_0(t) = A_0(t) cos(\phi_0(t)) = A_0(t) cos(\omega_0 t + \varphi(t, \omega_0)), \tag{6}$$

where, $\varphi(t, \omega_0)$ represents a function related to t and ω_0. A slow variation of $\varphi(t, \omega_0)$ causes the single-component signal with frequency ω_0 to move towards narrowband signals around frequency ω_0. Then, the IF of $x_0(t)$ can be defined as:

$$\hat{\omega}(t, \omega_0) = \partial_t \phi_0(t) = \omega_0 + \partial_t \varphi(t, \omega_0). \tag{7}$$

If $x(t)$ is expressed as $x(t) = \sum_{k=1}^{K} x_k(t)$, then the IF of $x(t)$ can be written as:

$$\hat{\omega}(t, \omega) = \omega + \partial_t \varphi(t, \omega). \tag{8}$$

According to the definition in (1), ST can be regarded as intercepting the signal $x(t)$ using a sliding window and then calculating the FT, thus, the IF of $ST(\tau, f)$ can be calculated as:

$$\hat{f}(\tau, f) = f + \frac{1}{2\pi} \partial_\tau arctan\left(\frac{\mathrm{Im}(ST(\tau, f))}{\mathrm{Re}(ST(\tau, f))}\right), \tag{9}$$

where, $\mathrm{Im}(ST(\tau, f))$ is the imaginary part of $ST(\tau, f)$ and $\mathrm{Re}(ST(\tau, f))$ is the real part. It should be noted that,

calculating IF through (9) will result in the information loss at the edge of the matrix. This is caused by replacing the derivative operation through difference operation. In addition, according to [21] [22] [23], the IF of $ST(\tau, f)$ also can be calculated as:

$$\hat{f}(\tau, f) = f + \mathrm{Re}\left\{\frac{\partial_\tau ST(\tau, f)}{j2\pi ST(\tau, f)}\right\}, \tag{10}$$

where, $j = \sqrt{-1}$. After obtaining the IF of $S(\tau, f)$, the first-order synchrosqueezed S-transform is defined as ([21] [23]):

$$SST\left(\tau, \hat{f}_l\right) = \int_{\mathbb{R}} |ST(\tau, f)|\, \delta\left(\hat{f}(\tau, f) - \hat{f}_l\right) df. \tag{11}$$

C. The novel IF algorithm

Both $\mathrm{Im}(ST(\tau, f))$ and $\mathrm{Re}(ST(\tau, f))$ can be considered as functions of τ and f. For convenience of expression, I and R will be used to represent $\mathrm{Im}(ST(\tau, f))$ and $\mathrm{Re}(ST(\tau, f))$, respectively. Based on (9), we have:

$$\begin{aligned}\partial_\tau arctan\left(\frac{I}{R}\right) &= \frac{1}{1 + I^2/R^2} \times \frac{R\partial_\tau I - I\partial_\tau R}{R^2} \\ &= \frac{R\partial_\tau I - I\partial_\tau R}{R^2 + I^2},\end{aligned} \tag{12}$$

where ∂_τ represents the partial derivative over τ. Thus, the proposed fast algorithm for IF calculation can be expressed as:

$$\hat{f}(\tau, f) = f + \frac{R\partial_\tau I - I\partial_\tau R}{2\pi(R^2 + I^2)}. \tag{13}$$

On the other hand, if (10) is expanded by complex division, the result is:

$$\frac{\partial_\tau ST(\tau, f)}{ST(\tau, f)} = \frac{R\partial_\tau R + I\partial_\tau I}{R^2 + I^2} + j\frac{R\partial_\tau I - I\partial_\tau R}{R^2 + I^2}. \tag{14}$$

Comparing (10) and (11) it can be found that:

$$\frac{R\partial_\tau I - I\partial_\tau R}{2\pi(R^2 + I^2)} = \mathrm{Re}\left\{\frac{\partial_\tau ST(\tau, f)}{j2\pi ST(\tau, f)}\right\}, \tag{15}$$

From which, it can be observed that the proposed algorithm is coherent with existing methods, and avoids unnecessary computational burden. However, whether calculating IF through (10) or (13), it is necessary to calculate the partial derivative of $ST(\tau, f)$ over τ. Writing $\partial_\tau ST(\tau, f)$ in the convolutional form:

$$\partial_\tau ST(\tau, f) = \int_{-\infty}^{+\infty} (x(t)e^{-j2\pi ft})\partial_\tau w(\tau - t, f)dt. \tag{16}$$

Combining the differential properties of convolution and FT, and changing (16) to the frequency domain:

$$\partial_\tau ST(\tau, f) = \int_{-\infty}^{+\infty} j2\pi\beta X(f + \beta)W(\beta, f)e^{j2\pi\beta\tau}d\beta. \tag{17}$$

The advantage of calculating $\partial_\tau ST(\tau, f)$ through (17) is that it avoids information loss at the edges and can be quickly calculated based on fast Fourier transform (FFT). At the same time, its expression is much more similar to ST.

D. Proposed amplitude-preserving SST

In the time domain, the integral of the ST's window function equals 1, and in the frequency domain, the maximum amplitude of the window function remains constant to preserve the accuracy of the S-transform's amplitude spectrum. However, owing to the variable resolution of the S-transform in the time-frequency domain, the width of the window in the frequency domain fluctuates, thereby impacting the accuracy of the amplitude after the synchrosqueezing operation. Consider a multi-component signal $s(t)$ defined as $s(t) = sin(2\pi 200t) + sin(2\pi 400t)$, the S-transform of $s(t)$ is shown in Fig.1(a). It should be noted that the amplitude of the ST's spectrum is half of the original signal, the results have shown are corrected.

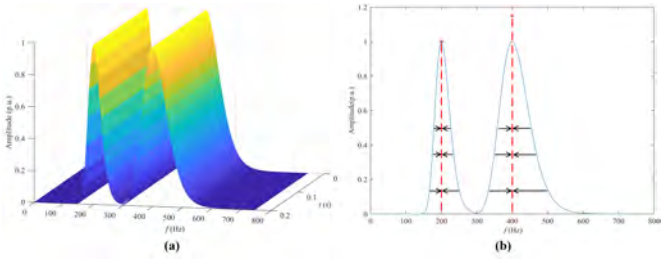

Fig. 1. (a) The S-transform of $s(t)$. (b) Illustration of synchrosqueezing operation.

From Fig.1(a), it can be observed that with the change of the window width, the amplitude spectrum's width of different signal components also changed. As shown in Fig. 1(b), synchrosqueezing operation based on the original S-transform will lead to amplitude distortion. To address this problem, an amplitude-preserving window is proposed. Conversely to (4), the amplitude-preserving window is defined in the frequency domain as:

$$\tilde{W}(\beta, f) = \sqrt{2\pi}\sigma(f)e^{-2\pi^2\beta^2\sigma(f)^2}. \tag{18}$$

For comparison, Fig. 2 shows the results of the original SST and amplitude-preserving SST of signal $s(t)$. It can be found that the original SST's amplitude spectrum has obvious distortion, while amplitude-preserving SST can maintain the accuracy of different signal components's amplitudes.

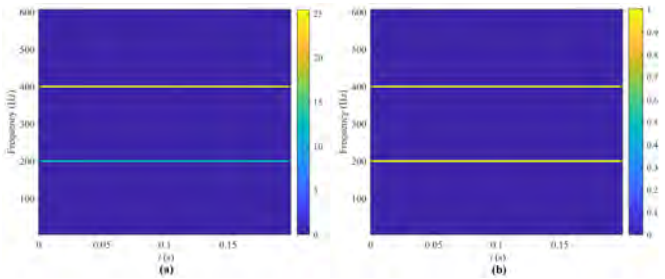

Fig. 2. (a) The results of original SST. (b) The results of amplitude-preserving SST.

It's important to highlight that when the window width undergoes minor changes, any amplitude distortion in the original SST can be subtle and challenging to detect. However, if the window width shifts significantly, the amplitude error

in the original SST becomes noticeable, particularly in applications sensitive to amplitude variations. The proposed amplitude-preserving SST effectively mitigates the influence of window width on amplitude, making it well-suited for power quality analysis.

III. The amplitude-preserving adaptive SST for power quality analysis

A. The adaptive window for power quality analysis

Based on IEEE standard 1159 [29], PQDs are categorized into seven main types, including transients, short-duration root-mean-square (rms) variations, long-duration rms variations, waveform distortion, and others. Given that the characteristic features of most power quality disturbance signals are concentrated around the power frequency, the detection of disturbances like swell, sag, and interruptions demands high time resolution. Conversely, harmonic and transient detection necessitate high frequency resolution. Hence, the adaptive window employed in this study is defined in the frequency domain as:

$$\begin{aligned} \tilde{W}(\beta, f) &= \sqrt{2\pi}(\lambda_1 f + \lambda_2) e^{-2\pi^2 \beta^2 (\lambda_1 f + \lambda_2)^2}, \\ s.t. &\lambda_1 \geq 0, \\ &\lambda_1 f + \lambda_2 > 0, \end{aligned} \tag{19}$$

where, λ_1 and λ_2 are the parameters to adjust the width of the adaptive window. The proposed adaptive window has high time resolution at low frequencies, which ensures the detection accuracy of time-sensitive information near the power frequency. At high frequencies, it has high frequency resolution, which can better locate disturbances such as harmonics and transients. After the synchrosqueezing operation, the overall frequency resolution will be further improved.

B. The discrete APASST

To analyze PQDs with APASST, it is necessary to introduce the discrete version of APASST. First, denote the discrete Fourier transform (DFT) of the discrete signal $x(n)$ as $X(n), n \in [0, N-1]$. When $n = 0$, it represents the direct-current (DC) component in the signal. As a special case, the DC component is equal to the mean value of the signal. The following discussion only includes the alternating-current (AC) component in the signal and the range of n is $n \in [1, N-1]$. Afterwards, a frequency shift operation on $X(n)$ is performed to obtain the matrix $\mathbf{X}(\mathbf{n}, \mathbf{m})$. For the discrete Fourier spectrum, this operation is a circular shift and the result is:

$$\mathbf{X}(\mathbf{n}, \mathbf{m}) = \begin{bmatrix} X(1) & X(2) & \cdots & X(M) \\ X(2) & X(3) & \cdots & X(M+1) \\ X(3) & X(4) & \cdots & X(M+2) \\ \vdots & \vdots & \cdots & \vdots \\ X(N-2) & X(N-1) & \cdots & X(M-2) \\ X(N-1) & X(1) & \cdots & X(M-1) \end{bmatrix}, \tag{20}$$

where, $M = N/2$. Then, (19) sampled in the frequency domain, is:

$$\tilde{W}(n, m) = \tilde{W}_{po}(n, m) + \tilde{W}_{ne}(n, m), \tag{21}$$

where, $\tilde{W}_{po}(n, m)$ and $\tilde{W}_{ne}(n, m)$ represent the positive and the negative frequency part of the spectrum, respectively. Then, $\tilde{W}_{po}(n, m)$ and $\tilde{W}_{ne}(n, m)$ can be calculated as:

$$\begin{cases} \tilde{W}_{po}(n, m) = \sqrt{2\pi}(\lambda_1 m + \lambda_2) e^{-2\pi^2 (n-1)^2 (\lambda_1 m + \lambda_2)^2}, \\ \tilde{W}_{ne}(n, m) = \sqrt{2\pi}(\lambda_1 m + \lambda_2) e^{-2\pi^2 (-N+n)^2 (\lambda_1 m + \lambda_2)^2}. \end{cases} \tag{22}$$

Writing $\tilde{W}(n, m)$ in matrix form:

$$\tilde{\mathbf{W}}(\mathbf{n}, \mathbf{m}) = \begin{bmatrix} \tilde{W}(1,1) & \cdots & \tilde{W}(1, M) \\ \tilde{W}(2,1) & \cdots & \tilde{W}(2, M) \\ \vdots & \cdots & \vdots \\ \tilde{W}(N-1,1) & \cdots & \tilde{W}(N-1, M) \end{bmatrix}. \tag{23}$$

Next, $ST(n, m)$ can be calculated as:

$$ST(n, m) = IDFT(\mathbf{X}(\mathbf{n}, \mathbf{m}) \odot \tilde{\mathbf{W}}(\mathbf{n}, \mathbf{m})), \tag{24}$$

where, $\odot$ is the entrywise product, and $IDFT$ denotes the inverse DFT. To calculate the partial derivative of $ST(n, m)$ over time, one must first calculate the derivative of the window function, which can be expressed in the frequency domain as:

$$\mathbf{D}\tilde{\mathbf{W}}(\mathbf{n}, \mathbf{m}) = 2\pi j \tilde{\mathbf{W}}(\mathbf{n}, \mathbf{m}) \odot \begin{bmatrix} 1 & \cdots & 1 \\ 2 & \cdots & 2 \\ \vdots & \cdots & \vdots \\ (N-1) & \cdots & (N-1) \end{bmatrix}. \tag{25}$$

After obtaining $\mathbf{D}\tilde{\mathbf{W}}(\mathbf{n}, \mathbf{m})$, $\partial_{\mathbf{n}}\mathbf{ST}(\mathbf{n}, \mathbf{m})$ can be calculated as:

$$\partial_{\mathbf{n}}\mathbf{ST}(\mathbf{n}, \mathbf{m}) = IDFT(\mathbf{X}(\mathbf{n}, \mathbf{m}) \odot \mathbf{D}\tilde{\mathbf{W}}(\mathbf{n}, \mathbf{m})). \tag{26}$$

Then, the IF matrix $\hat{f}(n, m)$ can be calculated using (13). It is worth noting that by comparing (12) and (13), it can be found that for a discrete signal of length N, calculating IF by (13) reduces $3N^2/2$ multiplication operations. Finally, the discrete APASST is obtained as:

$$APASST(n, \hat{m}_l) = \sum_{m: \left|\hat{f}(n,m) - \hat{m}_l\right| \leq \frac{\hat{m}_l}{2}} |\mathrm{ST}(n, m)| \tag{27}$$

C. Optimization of the APASST parameters

To select the optimal parameters of APASST, the chirp signal is first used as the test signal. The reason for choosing the chirp signal is that it has both time and frequency spans, which can balance the time and frequency resolution of APASST. Subsequently, the energy concentration is used to measure the performance of APASST under different parameters [30]. The advantage of energy concentration is that components of different concentrations within the same distribution have the same weight. For PQD analysis, this

is beneficial f or d istinguishing d ifferent s ignal components. Energy concentration can be calculated as follows:

$$\begin{cases} En = \sum_{m=1}^{M}\sum_{n=1}^{N}\left|\mathrm{TFD}_{\lambda_1,\lambda_2}(m,n)\right|^2, \\ \mathrm{nTFD}_{\lambda_1,\lambda_2}(m,n) = \frac{1}{En}\left|\mathrm{TFD}_{\lambda_1,\lambda_2}(m,n)\right|^2, \\ EC_{\lambda_1,\lambda_2} = \left(\sum_{m=1}^{M}\sum_{n=1}^{N}\sqrt{\left|\mathrm{nTFD}_{\lambda_1,\lambda_2}(m,n)\right|}\right)^2. \end{cases} \tag{28}$$

where, λ_1 and λ_2 are the parameters for adaptive conditional window width. $\mathrm{TFD}_{\lambda_1,\lambda_2}(m,n)$ represents TFD under the control of λ_1 and λ_2. En is the energy of $\mathrm{TFD}_{\lambda_1,\lambda_2}(m,n)$, and $\mathrm{nTFD}_{\lambda_1,\lambda_2}(m,n)$is the normalized $\mathrm{TFD}_{\lambda_1,\lambda_2}(m,n)$. EC_{λ_1,λ_2} is a measure of energy concentration, which is negatively correlated with the value of EC_{λ_1,λ_2}.

In (18), since the change of $\sigma(f)$ affects the width of the window in both time and frequency domain, to avoid energy leakage, $\sigma(f)$ is limited by the $3\sigma(f)$ rule of Gaussian window. Since APASST calculates the window function by (22), in the time domain, $\sigma(f)$ should satisfy

$$\sigma(f) \le \frac{N}{3}, \tag{29}$$

where, N represents the length of the signal. In the frequency domain, converting (18) into a standard Gaussian function form and obtain

$$\frac{1}{2\pi\sigma(f)} \le \frac{N}{3}. \tag{30}$$

Based on energy concentration, Particle Swarm Optimization (PSO) is used to optimize parameters. The reason for choosing PSO is that for multi-dimensional optimization, PSO has fewer parameters and faster convergence speed. Finally, the optimization problem can be described as

$$\begin{aligned} \arg\min_{\lambda_1,\lambda_2\in\mathbb{R}} & \left(\sum_{m=1}^{M}\sum_{n=1}^{N}\sqrt{\left|\mathrm{nTFD}_{\lambda_1,\lambda_2}(m,n)\right|}\right)^2, \\ \text{s.t. } & \lambda_1 \ge 0, \\ & \lambda_1 f + \lambda_2 > 0, \\ & \frac{3}{2\pi N} \le \sigma(f) \le \frac{N}{3}. \end{aligned} \tag{31}$$

After PSO optimization, λ_1 is set to 0.00008 and λ_2 is set to 0.05. It is worth noting that the purpose of using chirp signals as test signals is to obtain the optimal parameters of global equilibrium, so it can be applied to all types of PQDs.

IV. Validation of APASST method

In this section, various experiments were conducted to assess the performance of the proposed APASST. PQDs signals encompass time, frequency, and amplitude data, each requiring specific attention depending on the type of disturbance. For instance, in the case of harmonic disturbances, focus should be on harmonic frequency and amplitude, whereas for voltage interruptions, attention should be directed towards the start and end times of the interruptions. Additionally, to facilitate comparison, the results of OST [15] and IST [14] are included in the experiments, and the parameters of OST and IST were selected according to the recommended method.

To provide a quantitative evaluation of the detection outcomes, mean absolute error (MAE), mean square error (MSE), and root mean square error (RMSE) were simultaneously employed. These metrics are computed using the following equations:

$$\begin{cases} \mathrm{MSE} = \frac{1}{N}\sum_{i=1}^{N}\left(\hat{s}_i - s_i\right)^2, \\ \mathrm{MAE} = \frac{1}{N}\sum_{i=1}^{N}\left|\hat{s}_i - s_i\right|, \\ \mathrm{RMSE} = \sqrt{\frac{1}{N}\sum_{i=1}^{N}\left(\hat{s}_i - s_i\right)^2}, \end{cases} \tag{32}$$

where, $\hat{s}_i$ and s_i represent the i-th point of the measured value and the true value respectively, and N is the length of $\hat{s}_i$.

A. Detect harmonics and transient disturbances

In power systems, harmonics are one of the most common disturbances. According to the frequency of harmonics, harmonic disturbances can be divided into odd harmonics, even harmonics, and interharmonics. Among them, the frequencies of odd harmonics and even harmonics are odd or even multiples of the power frequency f_0, and the frequency of interharmonics is a non-integer multiple of f_0. In this case study, the test signal can be expressed as:

$$\begin{aligned} x(t) =& sin(2\pi f_0 t) + 0.4sin(6\times 2\pi f_0 t) \\ &+ 0.3sin(11\times 2\pi f_0 t) + 0.2sin(2\pi 780 t), \end{aligned} \tag{33}$$

where, the power frequency f_0 is 50 Hz, the time window is 0 to 0.2 s. $x(t)$ includes even harmonics, odd harmonics, and interharmonics. The results of OST, IST, and APASST are shown in Fig. 3. It can be found from Fig. 3 that all

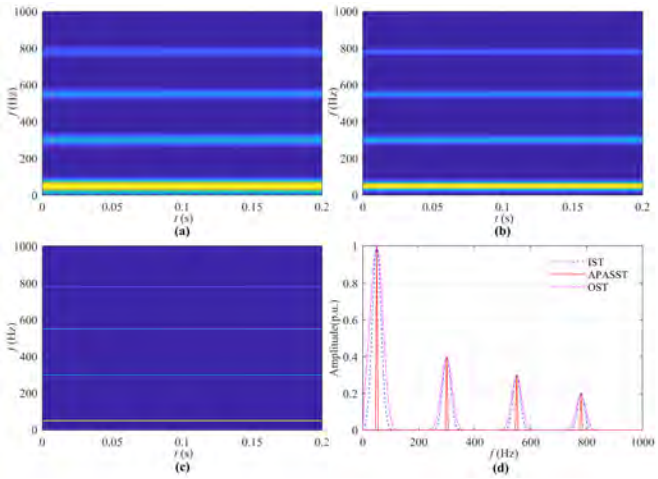

Fig. 3. (a) The results of OST. (b) The results of IST. (c) The results of APASST. (d) The frequency location details for OST, IST, and APASST.

three approaches can accurately measure the amplitudes of different signal components. IST has more accurate frequency localization than OST, this is because their window widths are adjusted through different strategies. While APASST can more accurately locate the frequencies of different components in both low and high frequencies.

Many events in the power network can cause oscillatory transient disturbances. Their mathematical model can be expressed as:

$$x(t) = sin(2\pi f_0 t) + p_1 e^{-p_2(t-t_1)} \left[u\left(t-t_1\right) - u\left(t-t_2\right)\right] sin\left(2\pi f_n t\right), \quad (34)$$

where, $u(t)$is the step function, p_1 and p_2 are amplitude parameters, f_n is the frequency of transient oscillation, t_1 and t_2 represent the start and end times respectively. In this case study, p_1 and p_2 are set to 0.5 and 10 respectively, and f_n is set to 10 f_0. t_1 is set to 0.1 s, t_2 is set to 0.15 s. The results of OST, IST, and APASST on oscillatory transient are shown in Fig. 4.

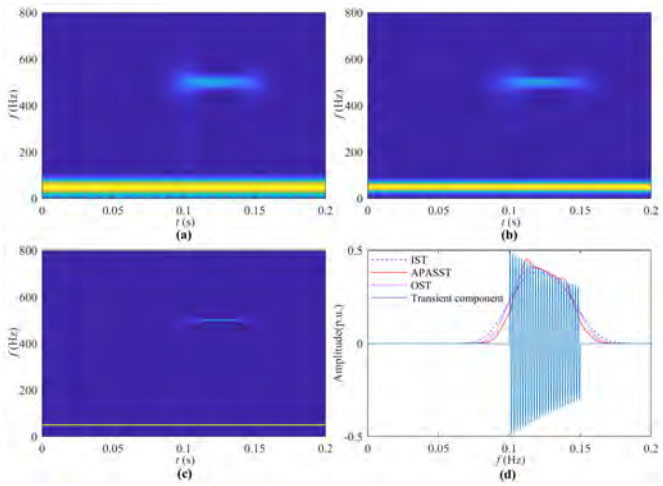

Fig. 4. (a) The results of OST. (b) The results of IST. (c) The results of APASST. (d) The amplitude details at frequency f_n extracted through OST, IST, and APASST.

In Fig.4, p.u. represents per unit. It can be observed that APASST has the highest accuracy in locating transients. Meanwhile, it can be found in Fig.4(b) that, the amplitude curve of APASST is not as smooth as OST and IST. This is because of the synchrosqueezing operation. To quantitatively compare the performance of different approaches, the amplitude error at frequency f_n and the frequency location error at 0.125 s of the transient component are listed in Table I.

TABLE I
THE AMPLITUDE ERROR AT FREQUENCY f_n AND THE FREQUENCY LOCATION ERROR AT 0.125 S

Approaches	Amplitude detect			Frequency locate		
	MAE	MSE	RMSE	MAE	MSE	RMSE
OST	0.029	0.004	0.062	0.019	0.005	0.071
IST	0.038	0.005	0.069	0.016	0.004	0.060
APASST	0.024	0.003	0.059	9.97×10^{-5}	2.49×10^{-7}	4.99×10^{-4}

From Table I, it can be found that the amplitude detection error of OST is smaller than IST, while the frequency locate performance of IST is better than OST. This is because the time resolution of OST at frequency f_n is better but the frequency resolution is worse. Among them, APASST has the best amplitude detection accuracy and can accurately locate the frequency and amplitude of transient disturbances.

B. Time-varying amplitude detection at power frequency

As defined in IEEE 1159 standard [29], voltage sag, interruption, swell, and voltage fluctuations are all represented by changes in amplitude at the power frequency f_0. For these disturbances, it is important that the time-frequency analysis approaches have good time resolution at the power frequency f_0. The voltage sag can be expressed as:

$$x(t) = sin(2\pi f_0 t)\left\{1 - p_3\left[u\left(t-t_1\right) - u\left(t-t_2\right)\right]\right\}, \quad (35)$$

where, t_1 is 0.06 s and t_2 is 0.12 s. p_3 represents the depth of voltage sag and it is set to 0.5. When $p_3 = 1$, it can represent an interruption. The voltage swell can be expressed as:

$$x(t) = sin(2\pi f_0 t)\left\{1 + p_4\left[u\left(t-t_1\right) - u\left(t-t_2\right)\right]\right\}, \quad (36)$$

where, t_1 is 0.08 s and t_2 is 0.15 s. p_4, set to 0.3, represents the amplitude of voltage swell. The voltage fluctuations can be expressed as:

$$x(t) = sin(2\pi f_0 t)\left[1 + p_5 sin(2\pi f_l t)\right], \quad (37)$$

where, p_5, set to 0.1, represents the amplitude of fluctuations. f_l, set to 10 Hz, is the frequency of the fluctuations. The detection results of the above four disturbances by OST, IST, and APASST are shown in Fig. 5 (the four graphs share the same legend).

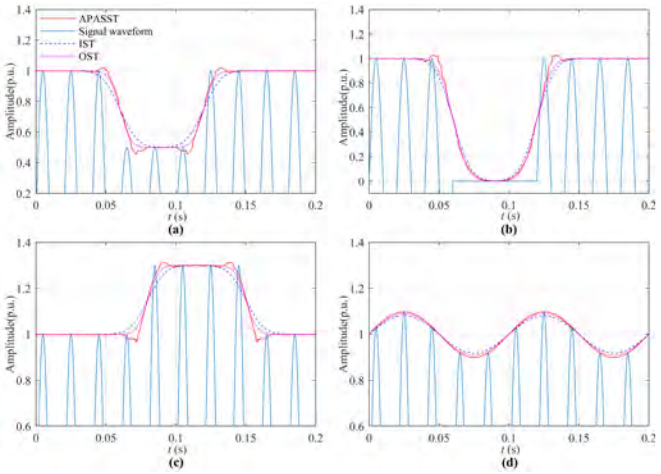

Fig. 5. (a) Amplitudes details of sag at frequency f_0. (b) Amplitudes details of interruption at frequency f_0. (c) Amplitude details of swell at frequency f_0. (d) Amplitudes details of voltage fluctuations at frequency f_0.

It can be found that APASST can better detect the time-varying amplitude at f_0. In Fig.5(a), (b), and (c), compared to OST and IST, the amplitude envelope of APASST is not smooth enough. This is due to the energy leakage being inevitable at the signal mutation point, and synchrosqueezing operation will cause the leaked energy to accumulate. To further compare their performance, Table II lists the errors of the three approaches.

It can be observed from Table II that although APASST is affected by energy leakage, it still maintains the minimum error. At the same time, APASST has the highest frequency locating accuracy.

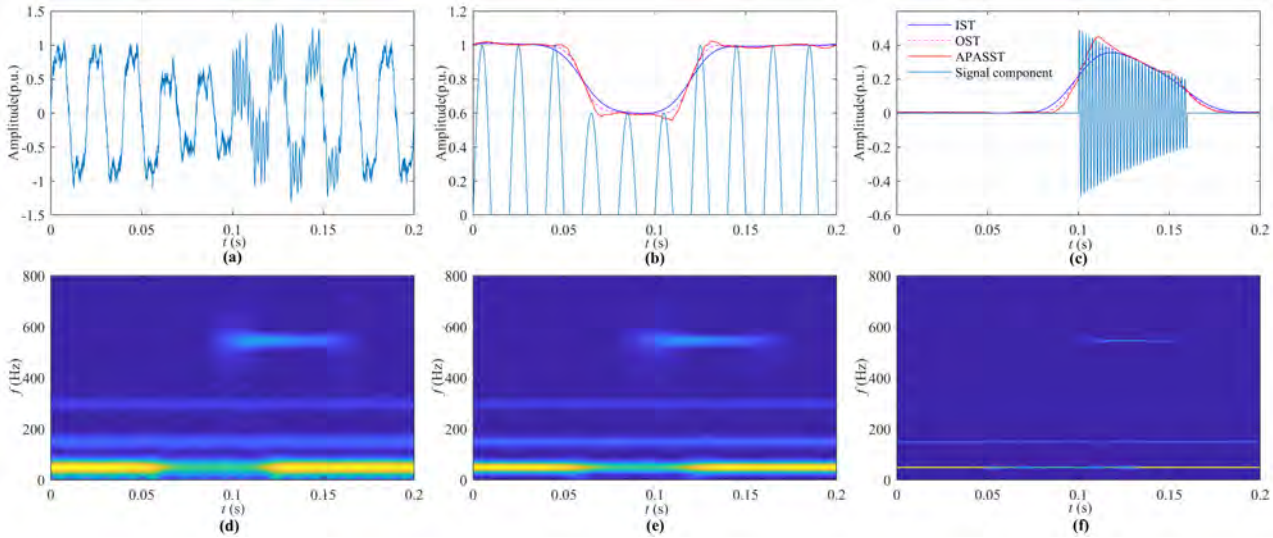

Fig. 6. Detection results of complex PQDs under 20 dB SNR. (a) The waveform of complex PQDs signal. (b) Sag detection results of IST, OST, and APASST. (c) Transients detection results of IST, OST, and APASST. (d) TFD of OST. (e) TFD of IST. (f) TFD of APASST.

TABLE II
TIME-VARYING AMPLITUDE DETECTION ERROR AT FREQUENCY f_0

PQDs	Approaches	MAE	MSE	RMSE
Sag	OST	0.026	0.004	0.061
	IST	0.040	0.006	0.076
	APASST	0.026	0.004	0.059
Interruption	OST	0.066	0.020	0.140
	IST	0.080	0.023	0.153
	APASST	0.064	0.020	0.137
Swell	OST	0.015	0.001	0.037
	IST	0.024	0.002	0.046
	APASST	0.014	0.001	0.033
Voltage fluctuations	OST	0.006	3.77×10^{-5}	0.006
	IST	0.012	1.72×10^{-4}	0.013
	APASST	0.005	3.33×10^{-5}	0.006

TABLE III
AMPLITUDE DETECTION ERROR OF PQDS COMPONENT UNDER DIFFERENT SNRS

SNR	Signal component	Approaches	MAE	MSE	RMSE
20 dB	Sag	OST	0.023	0.002	0.049
		IST	0.034	0.004	0.061
		APASST	0.022	0.002	0.047
	Transient	OST	0.028	0.003	0.056
		IST	0.036	0.004	0.064
		APASST	0.022	0.002	0.048
40 dB	Sag	OST	0.021	0.002	0.049
		IST	0.032	0.004	0.061
		APASST	0.021	0.002	0.046
	Transient	OST	0.026	0.003	0.056
		IST	0.033	0.004	0.064
		APASST	0.019	0.002	0.048

C. Complex disturbance parameter detection

Considering that various disturbances may overlap, resulting in complex disturbances, this case study further evaluates the performance of APASST. The selected test signal comprises a combination of sag, harmonics, and transients, encompassing multiple frequency components with simultaneous changes in amplitude. The sag component spans a period of 0.06 to 0.12 s, with an amplitude of 0.6 p.u. Harmonic components include the 3rd and 6th harmonics, with amplitudes of 0.2 and 0.1 p.u., respectively. The transient component operates at $12f_0$ frequency, with a duration of 0.1 to 0.16 s.

Moreover, to assess the noise resistance of APASST, Gaussian noise is introduced to the signal, yielding test signals with signal-to-noise ratios (SNR) of 20 dB and 40 dB. Fig. 6 illustrates the results for the signal at 20 dB SNR, while Table III presents the amplitude errors of sag and transient components at different SNRs.

Even at 20 dB SNR, APASST accurately identifies the frequencies of various disturbance components, as depicted in Fig. 6. Furthermore, Table III indicates that APASST exhibits minimal errors in detecting amplitude changes across both low-frequency and high-frequency components under different SNRs. This suggests that APASST maintains high time and frequency resolution while preserving amplitude detection accuracy.

D. Experimental tests

To further verify the performance of the proposed approach, experimental tests were performed with an ad-hoc measurement setup. The test signals are generated by Fluke 6105A, sampled by NI 9222, and then sent to the master computer for being analyzed. The measurement setup is shown in Fig. 7(a), and the accuracy parameters of the Fluke 6105A and the NI 9222 acquisition system can be found online.

As shown in Fig. 7(b) - (e), the experimental test was performed considering ‘interruption’, ‘interharmonics’,

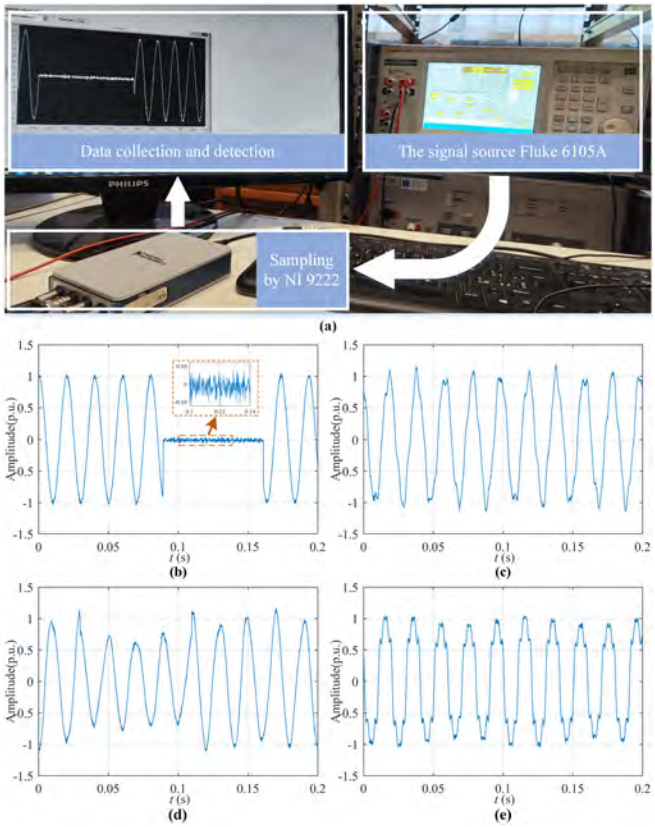

Fig. 7. (a) The structure of the test platform. (b) Example waveform of sampled 'interruption'. (c) Example waveform of sampled 'interharmonics'. (d) Example waveform of sampled complex disturbances 'sag+interharmonics'. (e) Example waveform of sampled complex disturbances 'flicker+harmonics'.

'sag+interharmonics', and 'flicker+harmonics' as test signals. These test signals include single and complex disturbances, as well as time-varying amplitudes at the power frequency and multiple frequency components. The sampling rate is 6400 Sa/s, the sampling period is 0.2 s, and the error is obtained by comparing the detection results with the parameter settings of Fluke 6105A. For all kinds of signals, test 20 times with different parameters each, and then calculate the average error of 20 tests.

The tests on the platform include noise interference non-integer period sampling and noise effects from the environment. In Fig. 7(b), it can be found that the amplitude of the noise is about 0.06 p.u., in other words, the SNR of the test signal is about 24.4 dB. Compared to simulation experiments where Gaussian noise is added to simulate the impact of noise, the signals sampled on the experimental platform can better validate the performance of the proposed approach. Fig. 8 shows the results of different approaches applied to two complex disturbances. Furthermore, Table IV lists the error evaluation of all test signals. For convenience, the complex disturbances 'sag+interharmonics' is denoted as 'C_1', and 'flicker+harmonics' is denoted as 'C_2'.

As can be seen from Fig. 8, OST and IST cannot completely separate the interharmonic components in C_1. Although APASST is affected by spectrum leakage, it can provide clear and readable interharmonic TFD. For C_2, all three approaches

TABLE IV
DETECTION ERROR OF DIFFERENT TEST SIGNALS

PQDs	Approaches	MAE	MSE	RMSE
Interruption	OST	0.091	0.029	0.171
	IST	0.136	0.044	0.209
	APASST	0.088	0.029	0.169
Interharmonics	OST	0.025	0.015	0.121
	IST	0.017	0.009	0.096
	APASST	3.14×10^{-4}	8.29×10^{-7}	9.1×10^{-4}
C_1 Sag	OST	0.029	0.002	0.042
	IST	0.028	0.002	0.047
	APASST	0.028	0.002	0.044
C_1 Interharmonics	OST	0.023	0.014	0.120
	IST	0.016	0.009	0.093
	APASST	6.21×10^{-4}	1.29×10^{-6}	0.004
C_2 Flicker	OST	0.005	4.19×10^{-5}	0.007
	IST	0.010	1.28×10^{-4}	0.011
	APASST	0.004	4.07×10^{-5}	0.006
C_2 Harmonics	OST	0.027	0.013	0.114
	IST	0.018	0.008	0.091
	APASST	4.49×10^{-4}	2.60×10^{-4}	0.016

can provide readable multi-component TFD, but APASST has the highest energy concentration.

In Table IV, by comparing 'interruption', 'C_1-sag' and 'C_2-flicker', it can be found that for time-varying amplitude detection at power frequency, IST has the worst performance, OST and APASST have similar performance, but APASST maintains the best. For multi-frequency locations, IST performs better than OST, but they are not as good as APASST. For 'interharmonics' and 'C_1-interharmonics', OST and IST maintain similar performance, while the RMSE of APASST changes from 9.1×10^{-4} to 0.004, which means that APASST is more susceptible to spectrum leakage caused by 'C_1-sag', but APASST still has the best performance.

In summary, the test results based on the power quality analysis platform indicate that IST or OST cannot simultaneously achieve high time and frequency resolution. The time resolution of OST is better than IST, while the frequency resolution of IST is better than OST. The performance of APASST is not as good as that in simulation experiments, but still has the highest accuracy in frequency localization and amplitude detection of multiple frequency components, meanwhile, APASST also maintains the best time resolution. For the PQDs signals with a period of 200 ms, the processing time of APASST is less than 150 ms, which means that APASST can process the PQDs signal in real time.

E. Discussion: APASST as a feature extraction approach for automatic classification of PQDs

The automatic classification of PQDs is a potential application scenario for APASST. In this part, the feature extraction capability of APASST for automatic classification of PQDs is explored. According to IEEE 1159 standard [29] and recent advanced methods, as listed in [31], simulation signals of 17 complex disturbances were generated. The SNR of signals is 20 dB, and each disturbance generates 2000 different samples. The sampling rate is 1600 Sa/s and the sampling

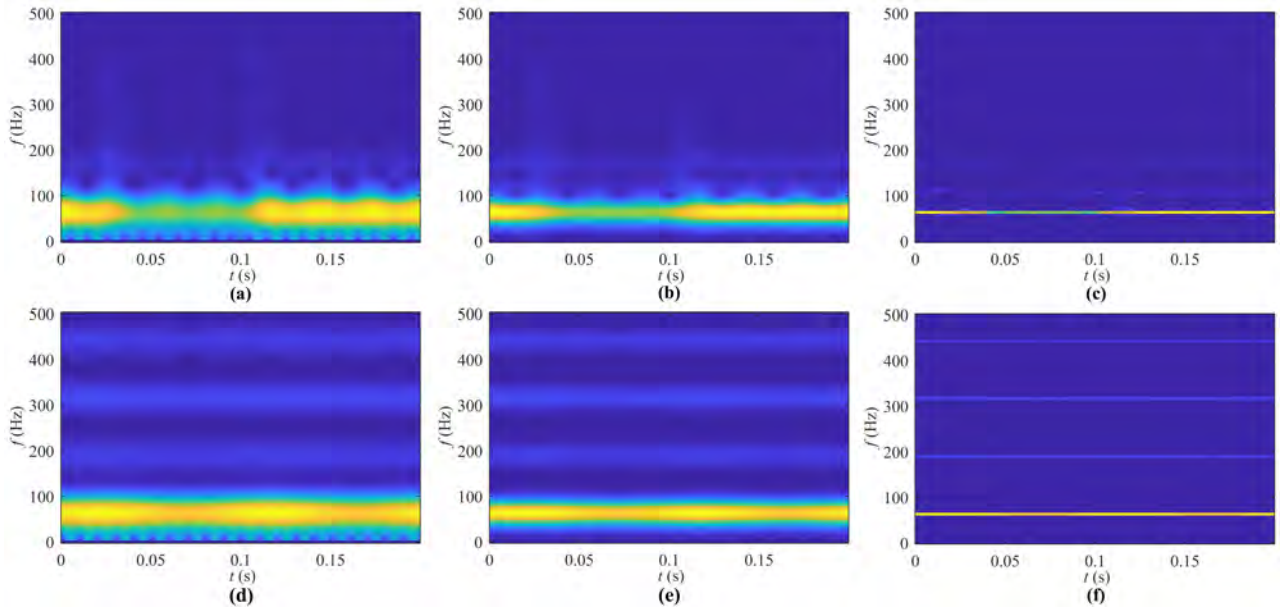

Fig. 8. (a) The OST result of C_1. (b) The IST result of C_1. (c) The APASST result of C_1. (d) The OST result of C_2. (e) The IST result of C_2. (f) The APASST result of C_2.

duration is 0.2 s. After time-frequency feature extraction by APASST, OST, and IST, ResNet18 is used as a classifier to identify disturbances. To verify the performance of different feature extraction approaches, the ratio of training data is set from 20 % to 60 %, and the results are listed in Table V.

TABLE V
RESULTS UNDER DIFFERENT TRAINING RATIOS

Approaches	Accuracy(%)				
	20%	30%	40%	50%	60%
OST	90.21	94.57	96.04	97.05	97.82
IST	91.17	94.88	96.73	97.17	97.86
APASST	92.24	95.35	97.05	97.97	98.24

It can be found that when using 60 % data for training, the performance of OST is close to that of IST, while APASST always maintains its advantage. Especially when the training data is only 40 %, the accuracy of APASST + ResNet18 is higher than 97 %, demonstrating good generalization performance. In [31], PHT+FTF + ResNet18 is used to identify 17 types of disturbances, and the accuracy is 97.37 % at 30 dB. In [32], DWT-AD + CNN is used to identify 16 types of disturbances, and the accuracy is 98.16 % at 20 dB. Compared with the above-advanced methods, APASST + ResNet18 achieved an accuracy of 98.24 % under 60 % training data, which means APASST can effectively extract disturbance features.

To further verify the feature extraction performance of APASST, based on the testing platform, 10 types of disturbances were sampled, with 50 samples collected for each disturbance. The classification results of APASST + ResNet18 are listed in Table VI. The test results have demonstrated the effectiveness of APASST's feature extraction capability on the test platform.

TABLE VI
THE PQDS CLASSIFICATION RESULT BASED ON FLUKE 6105A

PQD	Accuracy(%)	PQD	Accuracy(%)	Average(%)
Normal	100.00	Flicker	96.00	
Harmonics	100.00	Sag + harmonics	98.00	
Sag	98.00	Flicker + harmonics	96.00	98.00
Swell	98.00	Interrupt + harmonics	98.00	
Interrupt	100.00	Swell + harmonics	96.00	

V. CONCLUSION

This paper introduces a novel APASST, which defines a novel method for calculating the IF matrix. Compared to existing IF calculation methods, the proposed approach mitigates information loss at the matrix edge, at the same time, for a discrete signal of length N, $3N^2/2$ multiplication operations can be reduced. Simulation results demonstrate that APASST, utilizing frequency domain normalized windows, effectively circumvents the impact of window width changes on amplitude, accurately portraying the true amplitude of diverse signal components. The adaptive window mechanism equips APASST with the capability to sustain high time-frequency resolution across both low and high frequencies. Experiments conducted on single and complex disturbances attest to the ability of APASST to precisely detect the frequency and time-varying amplitude of PQDs signal components in real-time, even in the presence of substantial noise. Finally, experimental tests with an ad-hoc measurement setup confirm the exceptional performance of APASST.

The proposed APASST can provide high time-frequency resolution and accurate amplitude information, which is suitable for time-frequency analysis scenarios that require accurate amplitude mapping, such as power system fault

monitoring and fault finding, m echanical f ault diagnosis feature extraction, etc. In future work, the authors hope to achieve high-precision automatic classification of PQDs based on APASST, as well as specific P QDs p arameter detection such as short-term voltage changes.

REFERENCES

[1] P. Roy, J. He, T. Zhao, and Y. V. Singh, "Recent advances of wind-solar hybrid renewable energy systems for power generation: A review," *IEEE Open J. Ind. Electron. Soc.*, vol. 3, pp. 81–104, 2022.

[2] I. Ziyat, A. Gola, P. R. Palmer, S. Makonin, and F. Popowich, "Ev charging profiles and waveforms dataset (ev-cpw) and associated power quality analysis," *IEEE Access*, vol. 11, pp. 138 445–138 456, 2023.

[3] R. Narayanaswami, D. Sundaresan, and V. Ranjan Prema, "The mystery curve: A signal processing based power quality disturbance detection," *IEEE Trans. Ind. Electron.*, vol. 68, no. 10, pp. 10 078–10 086, 2021.

[4] J. Zhang, J. Song, C. Li, X. Xu, and H. Wen, "Novel frequency estimator for distorted power system signals using two-point iterative windowed dft," *IEEE Trans. Ind. Electron.*, pp. 1–12, 2024.

[5] D. Camarena-Martinez, M. Valtierra-Rodriguez, C. A. Perez-Ramirez, J. P. Amezquita-Sanchez, R. de Jesus Romero-Troncoso, and A. Garcia-Perez, "Novel downsampling empirical mode decomposition approach for power quality analysis," *IEEE Trans. Ind. Electron.*, vol. 63, no. 4, pp. 2369–2378, 2015.

[6] C. Zhao, K. Li, Y. Li, L. Wang, Y. Luo, X. Xu, X. Ding, and Q. Meng, "Novel method based on variational mode decomposition and a random discriminative projection extreme learning machine for multiple power quality disturbance recognition," *IEEE Trans. Ind. Informat.*, vol. 15, no. 5, pp. 2915–2926, 2018.

[7] K. Satpathi, Y. M. Yeap, A. Ukil, and N. Geddada, "Short-time fourier transform based transient analysis of vsc interfaced point-to-point dc system," *IEEE Trans. Ind. Electron.*, vol. 65, no. 5, pp. 4080–4091, 2017.

[8] Y. Yu, W. Zhao, S. Li, and S. Huang, "A two-stage wavelet decomposition method for instantaneous power quality indices estimation considering interharmonics and transient disturbances," *IEEE Trans. Instrum. Meas.*, vol. 70, pp. 1–13, 2021.

[9] H. Yuan, R. Du, X. Wang, X. Wei, and H. Dai, "Advanced online broadband impedance spectrum acquisition of fuel cells by s-transform," *IEEE Trans. Ind. Electron.*, vol. 70, no. 4, pp. 3740–3750, 2022.

[10] J. Li, H. Lin, Z. Teng, F. Zhang, and C. Liang, "Digital prolate spheroidal window-based s-transform for time-varying harmonic analysis," *Electr. Power Syst. Res.*, vol. 187, p. 106512, 2020.

[11] M. He, J. Ma, A. Mingotti, Q. Tang, L. Peretto, and Z. Teng, "An advanced diagnose framework for complex power quality disturbances using adaptive ks-transform and jetleaf synth network," *IEEE Trans. Ind. Electron.*, 2024.

[12] N. Singh and P. M. Pradhan, "Sharp detection of event's onset in seismic signals with asymmetrical kaiser window-based s-transform," *IEEE Geosci. Remote Sens. Lett.*, vol. 16, no. 10, pp. 1620–1624, 2019.

[13] J. Zhang, J. Li, S. Wang, W. Geng, and W. Cheng, "An improved unscale s-transform in frequency domain," *IEEE Geosci. Remote Sens. Lett.*, vol. 20, pp. 1–5, 2022.

[14] C. Liang, Z. Teng, J. Li, W. Yao, L. Wang, Q. He, and S. Hu, "Improved s-transform for time-frequency analysis for power quality disturbances," *IEEE Trans. Power Delivery*, vol. 37, no. 4, pp. 2942–2952, 2021.

[15] A. Moukadem, Z. Bouguila, D. O. Abdeslam, and A. Dieterlen, "A new optimized stockwell transform applied on synthetic and real non-stationary signals," *Digital Signal Process.*, vol. 46, pp. 226–238, 2015.

[16] M. V. Reddy and R. Sodhi, "A modified s-transform and random forests-based power quality assessment framework," *IEEE Trans. Instrum. Meas.*, vol. 67, no. 1, pp. 78–89, 2017.

[17] F. Auger and P. Flandrin, "Improving the readability of time-frequency and time-scale representations by the reassignment method," *IEEE Trans. Signal Process.*, vol. 43, no. 5, pp. 1068–1089, 1995.

[18] I. Daubechies, J. Lu, and H.-T. Wu, "Synchrosqueezed wavelet transforms: An empirical mode decomposition-like tool," *Appl. Comput. Harmon. Anal.*, vol. 30, no. 2, pp. 243–261, 2011.

[19] G. Thakur and H.-T. Wu, "Synchrosqueezing-based recovery of instantaneous frequency from nonuniform samples," *SIAM J. Math. Anal.*, vol. 43, no. 5, pp. 2078–2095, 2011.

[20] W. Bao, X. Tu, F. Li, and Y. Huang, "Generalized synchrosqueezing transform: Algorithm and applications," *IEEE Trans. Instrum. Meas.*, vol. 72, pp. 1–11, 2022.

[21] Z.-l. Huang, J. Zhang, T.-h. Zhao, and Y. Sun, "Synchrosqueezing s-transform and its application in seismic spectral decomposition," *IEEE Trans. Geosci. Remote Sens.*, vol. 54, no. 2, pp. 817–825, 2015.

[22] H. Yang, K. Zhang, Z. Jiang, X. Zhang, and Y. Xu, "Fault features diagnosis method of rolling bearing via optimized s synchroextracting transform," *IEEE Trans. Instrum. Meas.*, 2024.

[23] Y. Xu, L. Wang, G. Yu, and Y. Wang, "Generalized s-synchroextracting transform for fault diagnosis in rolling bearing," *IEEE Trans. Instrum. Meas.*, vol. 71, pp. 1–14, 2021.

[24] Y. Tao, S. Cao, Y. Ma, and M. Ma, "Second-order adaptive synchrosqueezing S transform and its application in seismic ground roll attenuation," *IEEE Geosci. Remote Sens. Lett.*, vol. 17, no. 8, pp. 1308–1312, 2019.

[25] D. Fourer and F. Auger, "Second-order horizontal synchrosqueezing of the s-transform: A specific wavelet case study," in *2020 28th European Signal Processing Conference (EUSIPCO)*. IEEE, 2021, pp. 2200–2204.

[26] W. Liu, Y. Liu, and S. Li, "Demodulated multisynchrosqueezing s transform for fault diagnosis of rotating machinery," *IEEE Sens. J.*, vol. 22, no. 21, pp. 20 773–20 784, 2022.

[27] K. Yu, X. Wang, and Y. Cheng, "A post-processing method for time-reassigned multisynchrosqueezing transform and its application in processing the strong frequency-varying signal," *IEEE Trans. Instrum. Meas.*, vol. 70, pp. 1–11, 2021.

[28] W. Liu, S. Cao, Z. Wang, K. Jiang, Q. Zhang, and Y. Chen, "A novel approach for seismic time-frequency analysis based on high-order synchrosqueezing transform," *IEEE Geosci. Remote Sens. Lett.*, vol. 15, no. 8, pp. 1159–1163, 2018.

[29] IEEE, "Ieee recommended practice for monitoring electric power quality; ieee std 1159-2009 (revision of ieee std 1159-1995)," 2009.

[30] L. Stanković, "A measure of some time–frequency distributions concentration," *Signal Processing*, vol. 81, no. 3, pp. 621–631, 2001.

[31] Y. Luo, K. Li, L. Li, J. Huang, C. Zhao, and X. Xiao, "A novel recognition method for complex power quality disturbances based on rotation vector and fuzzy transfer field," *IEEE Trans. Ind. Inf.*, 2024.

[32] D. Li, I. A. Channa, X. Chen, L. Dou, S. Khokhar, and N. Ab Azar, "A new deep learning method for classification of power quality disturbances using dwt-mra in utility smart grid," *Comput. Electr. Eng.*, vol. 117, p. 109290, 2024.

Kunzhi Zhu received the B.Sc. degree in measurement and control technology and instrument from Hunan University, Changsha, China, in 2018.

He is currently working toward the Ph.D. degree in electrical engineering, Hunan University, Changsha, China. His research interests include signal processing, machine learning, power system analysis, cyber-security of synchrophasor and mechanical fault diagnosis.

Zhaosheng Teng was born in Hunan, China, in 1963. He received the B.Sc., M.Sc., and Ph.D. degrees from Hunan University, Hunan, in 1984, 1995, and 1998, respectively, all in electrical engineering. He was a Post-Doctoral Research Fellow with the National University of Defense Technology, Hunan, from 1998 to 2000. Since 2000, he has been a Professor with Hunan University.

His current research interests include power quality monitoring, information fusion, and electrical measurement.

Alessandro Mingotti (S'17) was born in Cento (FE), Italy in 1992. He received the B.S., M.S., and Ph.D. degrees in electrical engineering from the University of Bologna, Bologna, Italy, in 2014, 2016, and 2020, respectively.

He is a Senior Assistant Professor at the University of Bologna from 2021. His research interests include management and condition maintenance of distribution networks, development, modelling, and metrological characterization of instrument transformers. He is also working on several National and European funded Projects.

Qiu Tang was born in Hunan, China, in 1970. She received the B.Sc., M.Sc., and Ph.D. degrees in electrical engineering from Hunan University, Changsha, China, in 1992, 1995, and 2010, respectively, and the M.Sc. degree in electrical engineering from the University of Nottingham, Nottingham, U.K., in 2005.

She has been an Associate Professor at Hunan University since 2006. Her current research interests include power system analysis, digital signal processing, and virtual instruments.

Lorenzo Peretto (M' 98, SM' 03) is currently a Professor of electrical and electronic measurements with the University of Bologna, Bologna, Italy. He has authored or co-authored more than 200 articles, holds 24 patents, and co-authored 3 books. He is a consultant of industries operating in the field of instrumentation and sensors for electrical measurements. His fields of research are the design and calibration of voltage and current instrument transformers (LPIT) for medium- and high-voltage power networks, the design and realization of calibration systems of voltage and current instrument transformers, and the measurements of electrical quantities in power networks.

Dr. Peretto is a member of the IEEE Instrumentation and Measurement Society. He is the Chairman of the Annual IEEE Applied Measurements for Power System Conference, a member of the IEC TC38 "Instrument Transformers," and the Chairman of the TC38/WG45 "Standard Mathematical Models for Instrument Transformers" and the TC38/WG53 "Uncertainty Evaluation in the Calibration of Instrument Transformers."